11 Macroscopic Fibers of Single-Wall Carbon Nanotubes

Virginia A. Davis and Matteo Pasquali

CONTENTS

11.1 INTRODUCTION

On the nano- to microscale, theoretical calculations and experimental measurements indicate that single-walled carbon nanotubes (SWNTs) have electrical conductivity and current-carrying capacity similar to copper [1,2], thermal conductivity higher than diamond [3,4], and mechanical strength higher than any naturally occurring or man-made material [5,6]. Although precise numbers are hard to pinpoint because of the limited accuracy of theoretical calculations and experiments on small bundles of nanotubes (NTs), Baughman et al. estimate a theoretical thermal conductivity of 2000 W/m K, an elastic modulus of 640 GPa, and a tensile strength of 37 GPa [7]. Some microelectronic and materials characterization applications (e.g., an atomic force microscopy tip) may be able to utilize the properties of individual and small

0-8493-1653-X/01/$0.00+$1.50

groups of SWNTs. However, many important applications require low-cost synthesis of SWNTs and manufacturing methods that preserve some or all of the nanoscale properties in a macroscopic object [8,9]. Whereas at least one solution to the economic mass-production of SWNTs is now available through the HiPco process [10] and potentially by other scalable routes [11,12], technologies for processing SWNTs into macroscopic materials are at a much earlier stage. Some of the most promising ones for manufacturing SWNT fibers are reviewed here.

Macroscopic carbon nanotube fibers have the potential to form high-strength, lightweight, thermally and electrically conducting structural elements at lower cost than other forms of SWNTs such as unaligned bucky paper [13]. Whereas futuristic applications such as space tethers and the space elevator [14] will require ultra-strong SWNT fibers, many other applications will require supplementary multifunctional properties and not such high mechanical strength [15]. The electrical properties may be used for highly efficient transmission of electricity over long distances. Thermal properties could be exploited in microelectronic applications where thermal management is an increasing problem as miniaturization progresses [14]. The extremely high surface area of SWNTs (above 300 m^2/g) could be exploited in carbon nanotube supercapacitors, electrochemically driven artificial muscles, hydrogen storage, and electrical energy harvesting [15]. Carbon nanotube fiber actuators have already been tested at temperatures in excess of 350°C with a maximum observed actuator stress of 26 MPa, which is roughly 100 times higher than natural muscle [7]. Potential uses include robots for planetary exploration and controlling blade pitch in jet engine rotors at temperatures above 1000°C [16].

Fibers containing SWNTs have been produced by four main types of processes: solid-state production or growth, electrophoretic processing, melt spinning, and solution spinning—i.e., liquid-state processing. Melt and solution spinning seem to be the most viable techniques for commercial scale-up; moreover continuous fibers consisting predominantly or solely of SWNTs have been produced only by solution spinning. This chapter emphasizes liquid-state processing and only briefly summarizes other techniques.

11.2 FIBERS PRODUCED DIRECTLY FROM SWNT SYNTHESIS

Fibers of carbon nanotubes micrometers to millimeters long have been produced by variations of chemical vapor deposition (CVD) [8,17,18]. For example, lengths up to 20 μm have been achieved using 1,3-dicyclohexylcarbodiimide to polymerize oxidized SWNTs into strands 50 to 150 nm in diameter [19]. Ribbons with preferential alignment (50–140 μm wide, 4–40 μm thick and 100 mm in length) have also been produced by heating oxidized acid-treated tubes at 100°C. Graphitization of the ribbons at 2200°C for 2 h under argon with a pressure of 0.5 MPa resulted in an increase of ribbon density from 1.1 to 1.5 g/cm^3 and an increase in Young's modulus from 24 to 60 GPa [20]. Electrical resistivity of as-grown ribbons was roughly 1 mΩ cm at room temperature.

On this microscale, alignment during tube growth can be enhanced by electric fields. Aligned SWNTs on the order of 10 μm can be grown under an electric field in the range of 0.5–2 V/μm [21]. Aligned CVD-grown nanotubes have been self-assembled into yarns up to 30 cm in length by drawing them out of arrays several hundred micrometers in height in a process similar to drawing silk out of a cocoon [22]; an array of 1 cm^2 area and 100 μm height could generate about 10 m of yarn. The diameter of the yarn can be controlled by the size of the drawing tool, with smaller tools generating smaller diameter yarns. The yarns were used to construct a light bulb filament and a polarizer suitable for use in the ultraviolet region.

Zhu et al. produced aligned strands up to 20 cm in length and several hundred micrometers in diameter using a floating catalyst method in a vertical furnace where n-hexane was catalytically pyrolyzed in the presence of a sulfur-containing compound and hydrogen. Typically, ferrocene-assisted CVD results in MWNTs at temperatures around 800°C and a mixture of SWNTs and MWNTs at temperatures above about 1000°C. The thiophene increased the yield of SWNTs; the temperature and flow rates were optimized to produce long SWNT strands in a continuous process [23]. The strands contained roughly 5 wt% iron and amorphous carbon impurities [23]. These strands were tweezed into smaller ones 5 to 20 μm in diameter. SEM showed a structural hierarchy in the fibers, which consisted of thousands of well-aligned bundles of SWNTs (diameter 1.1 to 1.7 nm) arranged in a two-dimensional triangular lattice. The volume fraction of SWNTs in the strands was estimated to be less than 48% based on the spacing between ropes measured by SEM. Raman spectroscopy showed that the dominant SWNT diameter was 1.1 nm. X-ray diffraction showed a full-width half-maximum (FWHM) of 44° [24]. Electrical resistivity on strands ranging in diameter from 50 μm to 0.5 mm was measured with a four-probe method. The crossover temperature (metallic to semiconducting) was approximately 90 K; from 90 to 300 K the behavior was metallic behavior with resistivity $\rho = 0.55$ to 0.7Ω cm [23]. Tensile testing was complicated by difficulties measuring the cross section of the strand (and thus the true stress) during testing. The starting diameter was measured by SEM and was in the range of 5–20 μm. The estimated Young's modulus ranged from 49 to 77 GPa. The authors assert that if one bases the Young's modulus on a cross section corresponding to a nanotube volume fraction of less than 48%, the result is 150 GPa, consistent with the modulus of SWNT bundles [23].

Li et al. have demonstrated the ability to continuously produce SWNT and MWNT fibers during chemical vapor deposition [25]. This process entails continuously winding an aerogel of high-purity nanotubes formed in the furnace hot zone onto a rotating rod. By changing the angle of the rod relative to the furnace axis, fibers with different degrees of twist can be produced. As with any chemical vapor deposition process, the reactor conditions can be controlled to produce either SWNTs or MWNTs; thus either SWNT or MWNT fibers can be produced by varying the reactor conditions. However, the SWNT fibers contain approximately 50 vol% impurities compared to approximately 10% for the MWNT fibers. Both types of fibers showed high degrees of alignment. Electrical resistivities as low as 0.12 mΩ cm were achieved. Mechanical strength varied from 0.1 to 1 GPa, assuming a typical carbon fiber density of 2 g/cc.[25]

11.3 ELECTROPHORETIC SPINNING

Gommans et al. have spun fibers electrophoretically from purified laser vaporization–grown SWNTs dispersed in n,n-dimethylformamide (DMF) at concentrations of about 0.01 mg/ml [26]. A commercially available carbon fiber (8 μm in diameter, about 12 mm long) was connected to a conducting wire (0.5 mm diameter, 10 mm long) with silver conducting paint. The wire was attached to a motor-driven stage via a pin vice. The carbon fiber translated along its axis into the suspension at a depth of a few millimeters. The carbon fiber was turned into a positive electrode by applying voltage, causing the SWNTs to migrate toward it and to form a cloud around the carbon fiber. SWNTs migrate because they are negatively charged in DMF and move electrophoretically toward the positively charged carbon fiber. As the carbon fiber was slowly withdrawn from the suspension, another fiber, attached to its end, spontaneously formed from the SWNT cloud. The fiber length was limited by the travel distance of the translation stage, the size of the SWNT cloud, and the smoothness of the withdrawal from the solution. Fibers were typically several centimeters long with diameters between 2 and 10 μm. The mass of SWNTs below the bath surface and the surface tension in the meniscus promoted the coalescence and axial alignment of bundles of SWNTs. Alignment was measured by polarized Raman spectroscopy and the axial versus perpendicular ratio was in the range of 2 to 6 [26].

11.4 CONVENTIONAL FIBER SPINNING

There are three main types of commercial fiber spinning processes (Fig. 11.1): melt spinning, dry solution spinning, and wet solution spinning [27]. Melt spinning is used to produce many polymer fibers, such as nylon and polyethylene terephthalate fibers, for commodity applications such as residential carpeting; it can be applied to single-component as well as composite fibers. In melt spinning, the fiber-forming material is melted and extruded under tension typically into cooled air; the rapid cooling induces the solidification of the fiber. Some polymer/SWNT composite fibers where polymer is the major constituent have been produced using this method. However, SWNTs decompose without melting at approximately 750°C in air and at approximately 2000°C in an inert atmosphere (e.g., argon); thus melt spinning is not a viable option for fibers where SWNTs are the sole component.

Most SWNT fibers have been produced by the solution spinning process. Solution spinning is more complicated than melt spinning because the solidification of the fiber involves additional steps: The fiber-forming material must be dissolved or finely dispersed into a solvent, and the solvent must be extracted after the extrusion to form the solid fiber. Therefore, solution spinning is typically used to produce fibers from materials that decompose before reaching their melting point or do not have a suitable viscosity for stable fiber formation. Solution spinning has been particularly effective for spinning fibers from stiff polymer molecules—e.g., poly(p-phenylene terephthalamide) (PPTA)—which form liquid crystals when dispersed in a solvent.

Several research groups have used solution spinning to produce bulk quantities of SWNT fibers (continuous lengths of 1 m or above). Solution spinning can be

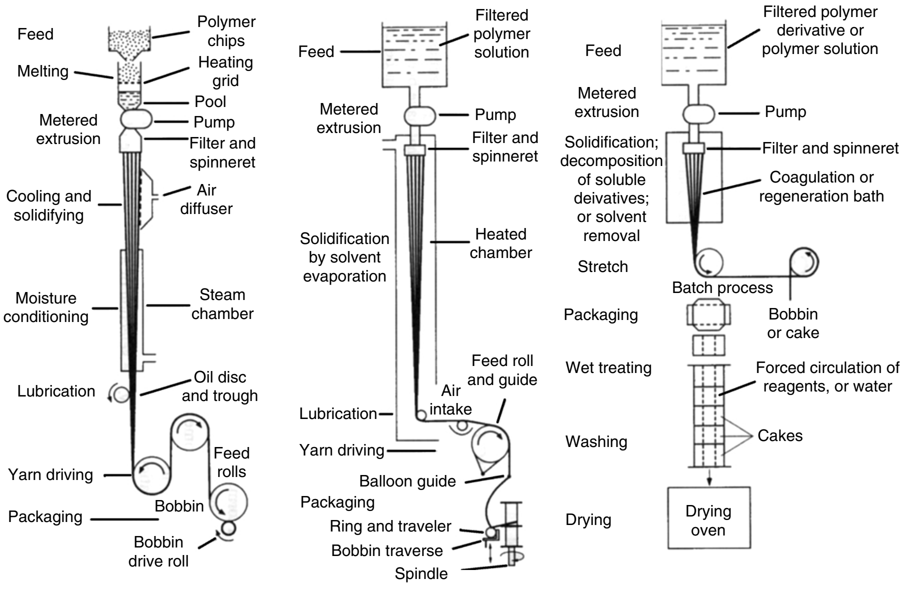

(a) Melt spinning (b) Dry spinning (c) Wet spinning

FIGURE 11.1 Three main types of spinning processes: melt spinning, dry solution spinning, and wet solution spinning [27].

considered as four-step process: (1) dispersion or dissolution of the fiber material into a solvent, (2) mixing and spinning the dispersion, (3) coagulation and drawing into a solid fiber, and (4) postprocessing of the fiber through subsequent washing, drying, or annealing steps.

Solution spinning can be divided into two main categories: dry solution spinning and wet solution spinning (Fig. 11.1). In both cases, the spinning solution consists of the polymer dissolved in a solvent. The solution is extruded through one or more small orifices in the spinneret and the solvent is removed, solidifying the fiber. Typically the polymer content is less than 30 wt% and sometimes less than 10 wt%. In many cases, the solution is formed at the molecular level. Dry spinning is used for systems such as cellulose acetate in acetone where the solvent is sufficiently volatile that it can be evaporated rapidly from the fiber during its formation. Wet spinning is used when the polymer is dissolved in a nonvolatile solvent that must be extracted by using another liquid that is miscible with the solvent but cannot dissolve the fiber-forming material. A key example of a wet solution–spun fiber is DuPont Kevlar™ (Wilmington, DA), produced from poly(p-phenylene terephthalamide) (PPTA) dissolved in sulfuric acid. In wet solution spinning (Fig. 11.1), the solution typically goes through an air (or inert gas) gap and then enters the coagulation bath. In this case, the process is termed dry-jet wet spinning. The air gap allows elongation and cooling of the spinning solution prior to coagulation. The presence and length of the air gap depends on the ability of the polymer solution exiting the spinneret to withstand surface forces prior to entering the coagulation bath.

Liquid filaments are unstable to surface waves, which are amplified by surface tension (Rayleigh instability) [28]; higher surface tension and small filament diameters promote the growth of the waves and the eventual breakup of the filament into droplets, whereas viscous forces delay the development of the instability. High-viscosity fibers as well as thicker fibers can normally support a larger air gap, particularly if the polymer is extension-thickening—i.e., its viscosity in extension grows with strain rate. Typical air gaps used in PPTA spinning are less than 2 cm; a gap of 0.5 to 1.5 cm is considered optimal [29]. If larger gaps are used, the (liquid) fiber breaks before entering the coagulation bath. In contrast, higher viscosity poly(p-phenylene benzobisthiazole) (PBZT)/poly(phosphoric acid) and (p-phenylene benzobisoxazole) (PBO)/poly(phosphoric acid) spinning solutions can support air gaps of up to 20 cm without fiber line breakage [29]. If the fiber cannot support an air gap at all, the spinneret is immersed directly into the coagulation bath and the process is termed wet-jet wet spinning.

Upon entering the coagulation bath, mass transfer occurs between the coagulant (nonsolvent) in the bath and the solvent in the spinning solution, which can now be considered the protofiber [30,31]. The goal of the coagulation process is to freeze the structure of the protofiber and solidify the fiber. The final properties of the resulting fiber depend on the initial polymer solution, the coagulation process [29,32–35], drawing of the fiber, and postprocessing steps such as secondary washing [29,34] or drying [36] of the fiber.

The first step of the solution spinning process, dispersal into a solvent, is far from trivial for SWNTs [7]. Due to high van der Waals interactions, it is typically only possible to disperse <0.5 wt% of SWNT in small molecule organic solvents such as dichlorobenzene or aqueous solutions of surfactants such as sodium dodecyl sulfate (SDS), although recent work has shown that strong acids can disperse SWNTs at higher concentration [37–39]. Current research on SWNT functionalization and wrapping may provide new means for dissolving higher concentrations of SWNTs in these liquids for fiber production [40–43].

Finding an appropriate dispersion for the SWNTs is not sufficient for producing high-quality fibers; understanding the phase behavior of the dispersion is critical [15,37,44,45]. The phase behavior and the related rheological properties of the dispersion profoundly influence the selection of the spinning solution concentration, spinning and coagulation process variables, and alignment in the as-spun fibers. Ultimate fiber properties are determined by these variables as well as subsequent washing, drawing, drying, and annealing processes [46].

11.4.1 MELT-SPUN COMPOSITE FIBERS

Reinforcement of existing materials with nanomaterials including SWNTs is a topic of significant current interest because relatively low loadings of the costly component (SWNTs) could yield significant improvements in properties. Improvements in electrical and thermal conductivity are of particular interest, although mechanical reinforcement is also an important application. As with the development of other SWNT materials, this field is still in its infancy; current results should be viewed as preliminary and not indicative of the full potential of SWNT composite fibers.

Some of the first melt spun composite SWNT fibers were produced by Andrews et al. using carbon pitch as the main component [47]. SWNTs from Carbolex, Inc. (Lexington, KY) were purified and mixed with isotropic petroleum pitch in quinoline. After sonication and solvent removal, the fibers were melt spun, drawn, and put through a two-stage heat treatment in air and nitrogen. Mixtures containing 8 and 10 wt% SWNT yielded fibers that were too weak to be collected; however, fibers produced with 1 wt% and 5 wt% SWNTs showed improved mechanical and electrical properties. Improvements were a 90% increase in tensile strength, a 150% increase in elastic modulus, and a 70% drop in electrical resistivity (Table 11.1).

Haggenmueller et al. produced SWNT polymethylmethacrylate (PMMA) films and fibers [48]. Three types of SWNT were investigated: raw and purified soot from laser ablation, and Tubes@Rice material. The SWNTs were dispersed in PMMA (M_w = 10,000) in dimethyl formamide (DMF) by prolonged sonication. After evaporation of the DMF, the resulting SWNT/PMMA pellets were melt mixed, spun from a 600-µm orifice, and drawn under tension by a windup spool at high speed. The maximum draw ratio (defined as $\lambda = (D_o/D)^2$) ranged from 60 to 3600, corresponding to fiber diameters between 75 and 10 µm, respectively. Increasing SWNT content dramatically increased the melt viscosity; this resulted in melt fracture evidenced by surface roughness, striations along the fiber axis, and nonuniform diameter. Increasing the SWNT weight fraction also decreased the attainable draw ratios and increased the frequency of fiber breaks; fibers were successfully produced from loadings up to 8 wt% SWNT. The 10 wt% SWNT mixture was too viscous to be extruded. Mechanical and electrical properties depended on SWNT concentration and draw ratio. For melt-pressed films, at a draw ratio of $\lambda = 4$, the electrical resistivity in the direction parallel to processing decreased approximately 100-fold from 8.5 m at 1.3 wt% SWNT to 0.087 Ωm at 6.6 wt%. In the direction perpendicular to processing, the electrical resistivities were only slightly higher: 12.8 and 0.14 Ωm, respectively. The fibers were highly anisotropic; their conductivity was below the detection limit, in agreement with the fact that weight fraction of SWNTs for percolation increases as the nanotubes align. At a draw ratio of $\lambda = 70$, the elastic modulus G increased from 3.1 GPa in the absence of SWNT to 6 GPa for 8 wt% SWNT. The draw ratio had a small effect on the modulus but significantly affected the yield stress. In fibers containing 5 wt% purified SWNT soot, the yield stress doubled from 65 to 130 MPa as the draw ratio was raised from $\lambda = 40$ to 300. Similar results were observed with the other types of SWNTs. These improvements

TABLE 11.1
Properties of SWNT/Pitch Fibers [45,47]

Sample	Tensile Strength [MPa]	Elastic Modulus [GPa]	Electrical Resistivity [m••cm]
Pitch	480	33	8.4
Pitch/1 wt% SWNTs	620	41	2.5
Pitch/5 wt% SWNTs	850	77	2.2

are consistent with the high degree of alignment measured by polarized Raman spectroscopy at multiple angles relative to the fiber axis; a fiber containing 1 wt% purified soot had a FWHM = 4° [48].

Efforts to incorporate SWNTs into polypropylene (PP) fibers have built on earlier success in incorporating carbon nanofibers into PP [49–52]. Bhattacharyya et al. [53] produced 0.8 wt% SWNT-PP fibers using HiPco SWNTs and melt flow index (MFI) of 17 polypropylene. The SWNTs were purified (less than 1 wt% impurities) using methods found in the literature [54], mixed with the PP in a Haake Rheomix 600 at 240°C, and filtered to remove the largest aggregates. This preparation procedure, however, failed to disperse satisfactorily the SWNTs, which remained clumped into domains of tens of micrometers. The SWNTs were found to promote faster PP crystallization, probably by acting as nucleation sites, and to yield smaller PP crystallites. The SWNTs in the final fiber were better oriented axially than the PP. Mechanical properties were largely unaffected by the presence of the SWNTs as a result of the poor dispersion. The mechanical properties are expected to improve as better methods for dispersing the SWNTs in PP are found.

11.4.2 SOLUTION-SPUN SWNT FIBERS

11.4.2.1 SWNT/Liquid Crystalline Polymer Composite Fibers

Improving the properties of high-performance fibers such as poly(p-phenylene benxobisthiazole) (PBO) through the incorporation of SWNTs is an important potential application of SWNTs. Commercial PBO fiber (Zylon™) is one of the strongest fibers with a tensile strength of 5.8 GPa [55]. Kumar et al. [56] synthesized PBO in poly(phosphoric acid) (PPA) in the presence of purified HiPco SWNTs at concentrations of 0, 5, and 10 wt%. Optical microscopy showed that the SWNTs were well dispersed in the liquid crystalline PBO/PPA solution. The liquid crystalline solution was dry-jet wet spun into a water coagulation gap with an air gap of 10 cm and draw ratios as high as 10. SWNT loading improved modulus, tensile strength, and elongation to break. For 10 wt% the improvements were 20, 60, and 40%, respectively (Table 11.2). Achieving similar improvements with commercial Zylon™ fibers (twice as strong as the laboratory control) could yield fibers with a tensile strength in excess of 8 GPa. Very importantly the incorporation of SWNTs improved the compressive strength of the fibers. The coefficient

TABLE 11.2
Mechanical Properties of SWNT/PBO Fibers [56]

Sample	Tensile Modulus (GPa)	Strain to Failure (%)	Tensile Strength (GPa)	Compressive Strength (GPa)
PBO	138 ± 20	2.0 ± 0.2	2.6 ± 0.3	0.35 ± 0.6
PBO/5 wt% SWNTs	156 ± 20	2.3 ± 0.3	3.2 ± 0.3	0.4 ± 0.6
PBO/10 wt% SWNTs	167 ± 15	2.8 ± 0.3	4.2 ± 0.5	0.50 ± 0.6

of thermal expansion dropped from −6 ppm/K for the pure PBO fiber to −4 ppm/K at 10% SWNT loading. Thermal degradation was not affected by the presence of SWNTs. The degree of alignment of the PBO in the fiber was also unaffected by the SWNTs. The electrical conductivity was below the limit of detection. The authors state that such low conductivity indicates both good dispersion and strong alignment; however, either one of these two morphological features would suffice to explain the lack of conductivity, because 10 vol% is well below the percolation threshold of aligned slender anisotropic objects as well as randomly packed isotropic ones [57].

Polyacrylonitrile (PAN) copolymers are used as carbon fiber precursors and for developing porous activated carbon that can be used in various applications (e.g., catalysis, electrochemistry, separations, and energy storage). Sreekumar et al. [58] produced PAN/SWNT fibers by dry-jet wet solution spinning. Composite fibers with 10 wt% SWNT had dramatically better properties than the pure PAN fibers. The tensile modulus nearly doubled from 7.9 GPa (pure PAN fiber) to 14.2 GPa (5 wt% SWNT fiber) and 16.2 GPa (10 wt% SWNT fiber). Tensile strength was not improved as much: The pure PAN fiber had a strength of 0.23 GPa and the 5% and 10% fibers had strengths of 0.36 GPa and 0.33 GPa, respectively. All fibers showed similar elongation at break (about 10%). The presence of SWNTs improved thermal stability. The glass transition temperature grew from 103°C (pure fiber) to 114°C (5 wt% fiber) to 143°C (10 wt% SWNT). The SWNT/PAN fibers retained their elastic modulus better than the pure PAN fibers at high temperature. (Interestingly the 5% SWNT fibers retained modulus better than the 10% fibers.) At 200°C, thermal shrinkage of the 10% fiber was nearly half that of the control. Supercapacitor films of SWNT/PAN were produced by a similar dispersion technique followed by film casting in vacuum [59].

11.4.2.2 Fibers Produced from SWNT/Surfactant Dispersions

The first truly scalable continuous process for making fibers composed primarily or solely of SWNTs was developed by a team at the Centre National de la Reserche Scientifique (CNRS) and the Université Bordeaux [60,61]. This process produces fibers composed by a network of SWNTs and a polymer, typically polyvinyl alcohol (PVA). The SWNTs are dispersed in an aqueous solution with the aid of surfactants and then injected into a flowing polymer (PVA) solution. The polymer can be removed by washing the fiber repeatedly and by heating the fiber at temperatures between the decomposition temperature of the polymer and that of the SWNTs. The original process developed at CNRS employs a rotating polymer solution bath mounted on a turntable [60–62]; a modified process developed by the University of Texas at Dallas uses a coflowing stream of polymer solution [63,64].

SWNT suspensions are analogous to solutions of rod-like polymers or anisotropic colloids [44]. Just as the nature of surfactants plays a critical role in the phase behavior of classical colloids, the same is true for nanotubes. In the CNRS process, SWNTs were sonicated in aqueous solutions of sodium dodecyl sulfate (SDS), an anionic surfactant that adsorbs at the surface of SWNT bundles. Similar adsorption behavior has also been observed with cationic surfactants such as tetratrimethylamonium bromide.

Vigolo et al. [44,61] studied the phase behavior of SWNTs produced by electric arc, laser vaporization, and HiPco in SDS in order to identify the ranges of surfactant and SWNT concentration that yielded dispersions with optimal processability. The stabilization mechanism seems to be a balance between repulsive electrostatic forces induced by the charged groups on the surfactants and attractive forces induced by van der Waals forces between SWNTs (or bundles of SWNTs) and by micellar depletion.

At low surfactant concentration, the number of surfactant molecules adsorbed on the SWNTs, which are present in small bundles after sonication, is not sufficient to counterbalance the long-range van der Waals forces—van der Waals forces between parallel cylinders decay with $r^{-1.5}$, where r is the separation between the cylinders [65]. Therefore, the bundles stick back together after sonication and form large dense clusters. At high surfactant concentration, the excess surfactant that is not adsorbed on the SWNT bundles forms nanometer-sized micelles. As two SWNT bundles approach each other, they exclude micelles; this produces a difference of osmotic pressure [65,66], which in effect brings the bundles closer together and causes the formation of flocs that coexist with well-dispersed thin bundles [44]. The proportion of clusters grows with surfactant concentration.

At intermediate SDS concentrations the system forms an apparently homogeneous phase of well-dispersed small bundles. In the case of electric arc–produced SWNTs, this homogeneous phase exists up to approximately 0.35 wt% SWNT in 1 wt% SDS. Similar behavior was observed for SWNTs produced by all three production methods, but the exact phase boundaries were dependent on the production technique; the boundaries shifted to higher concentrations for the HiPco-produced SWNTs, probably because of differences in length and diameter distributions. The homogeneous dispersions with the highest content of SWNTs showed optimal processability, although fibers of HiPco SWNTs could be produced also from nonhomogeneous dispersions [44]. The origin of the SWNTs also influenced the ribbon/fiber morphology. For HiPco-produced tubes, a smaller weight fraction (approximately 0.15 wt%) was needed to make homogeneous fibers with a uniform and nearly cylindrical cross section [62]. HiPco tubes also yielded stable fiber formation and good mechanical properties at higher velocities [60].

Due to their anisotropy, SWNTs align in shear or elongational flow. Injecting the SWNT dispersion in a coflowing stream of polymer has two beneficial effects on the fiber formation. It aligns the SWNTs by imposing a small amount of extensional flow on the protofiber that can be controlled by the mismatch between the velocity of the SWNT dispersion being injected and the velocity of the polymeric bath. Moreover the rotating bath supports and transports the protofiber during the early stages of coagulation, while it is still too weak to support an applied tension. If the coagulation bath were not moving, the fiber would have to be drawn mechanically through the coagulation bath, which is not possible unless the liquid filament has a high enough viscosity and the ability to withstand tension along the streamlines (usually associated with extensional thickening). Most of the surfactant leaves the filament during the coagulation, while at the same time the PVA molecules penetrate the forming fiber and stabilize it by forming bridges with the SWNTs [61,62]. The SWNT/SDS dispersions were injected through a 0.5 mm–diameter syringe needle into a rotating bath containing 2 to 6 wt% of PVA (M_w 70,000 hydrolysis 89% solution viscosity, about 200 cp) [44,60,61]. Amphiphilic polymers such as PVA are ineffective at stabilizing SWNTs; they stick to each other almost as soon as they enter the bath. This can be considered as coagulation through bridging flocculation [62]. Polarized optical microscopy of ribbons suspended in water showed that there is preferential alignment along the ribbon axis. SEM shows preferential axial alignment in the cleaned dry ribbons although the dried ribbons displayed weaker anisotropy than the ribbons suspended in water. Low-viscosity PVA solutions yield fibers with lower alignment, possibly because they are less effective at rapidly stretching the extruded filament.

Au: Correct?

High strain rates in the processing flow yielded better aligned as-spun fibers [60]. The relevant quantities include the shear rate in the syringe tube, the ratio of the viscosity of the coagulant and SWNT dispersion, and the ratio between the coagulant velocity and the extrusion speed of the SWNT dispersion. The shear rate in the syringe tube should promote axial alignment of the SWNT bundles before they meet the PVA solution. A higher coagulant/SWNT dispersion viscosity ratio should accelerate the filament over a smaller distance, i.e., produce a higher rate of extension immediately after the syringe orifice. The ratio of the velocity of the rotating PVA bath and the extruded SWNT dispersion controls the total extensional strain that is experienced by the filament as it coagulates into a ribbon [60]. However, variations in polymer solution speed between 300–800 m/h and the SWNT dispersion injection rate (35–100 ml/hr) did not affect the orientation in the dried fibers. This suggests that alignment is fixed during the drying stage and not during the initial coagulation process [62].

The fibers from the CNRS process possess a hierarchical structure with well-developed porosity and high surface area (160 m^2/g by the Brunauer-Emmett-Teller (BET) method, compared to 200 m^2/g of standard bucky paper) [67]. This makes them of interest for nanofluidic devices, adsorbents and absorbents, catalysis support, and host systems for encapsulation of biomolecules for sensors, smart textiles, and other nanotechnologies in which wetting and sorption properties play an important role. Cross sections of fibers dried under tension reveal a well-defined core consisting mostly of SWNTs and a shell that contains most of the carbon impurities; such impurities were randomly distributed in the initial fibers. Thus separation occurred as the fibers collapsed and this may provide a means of large-scale SWNT purification. Chemical irradiative or thermal removal of the shell would result in purified SWNTs [61].

Neimark et al. [67,68] made a detailed study of the fiber morphology and gas adsorption. Gas adsorption measurements were made on fibers that had been heated in air at 320°C for 3 hours. This removed 95% of the organic species while keeping the fibers intact. The fibers have several levels of structural organization; 10–50-μm fibers are composed of straight elementary filaments 0.2 to 2 μm in diameter with a hairy surface [67]. These elementary filaments consist of densely aligned nanotube bundles 10–30 nm in diameter, which in turn consist of SWNTs 1–2 nm in diameter. The elementary filaments are aligned in a close-packed configuration in the fiber skin of 1–5 μm diameter, while the core consists of a nanofelt of loosely packed bundles; the skin-core morphology resembles that of polyacrylonitrile (PAN)–based carbon fibers. This was confirmed by comparing alignment measured by x-ray scattering and polarized Raman spectroscopy. In x-ray scattering, where the whole fiber is exposed to radiation, the FWHM was 75°. In polarized Raman spectroscopy, where a limited boundary layer of about 1 μm is probed, the FWHM was about 35°; this indicates the surface alignment is much better than the alignment in the core.

The original CNRS process resulted in fibers that showed a plastic deformation before breaking and could be curved through 360° within a length of tens of micrometers, demonstrating that the fibers are more flexible and resistant to torsion compared to classical carbon fibers [61]. Four-probe electrical resistivity measurements gave a room temperature resistivity of approximately 0.1 Ω cm and a nonmetallic behavior when the temperature was decreased. This value was influenced by the presence of the polymer and carbon impurities; it is three orders of magnitude higher than that of small bundles of SWNTs [61]. In an improvement to the original process, the washed and dried fibers are rewetted, swollen, and dried under tensile load with a weight attached to one end of the fiber. They can be stretched up to 160% and do not disassemble even in solvents where the polymer is highly soluble. This suggests that the SWNTs and adsorbed polymer form an effectively cross-linked network that can be easily deformed [62]. The qualitative effect of stretching on fiber morphology and alignment can be seen in Fig. 11.2. This effect can be quantified by the change in FWHM—from 75 to 80° for raw fibers to less than 50° for fibers with draw ratios of 125% or greater. At higher draw ratios, the SWNTs seemed to slide and unbind from the PVA; both the applied stress needed to achieve the higher draw ratio and the FWHM remained constant. The improvement in alignment with stretching translated into improved mechanical properties: The Young's modulus increased fourfold from about 10 GPa for the raw fibers to 40 GPa for fibers stretched 145% in water with a load of 0.44 g. The tensile strength of these fibers increased from 125 MPa to 230 MPa, respectively. The effectiveness of the stretching process was found to be dependent on the liquid used to rewet the fiber; poorer PVA solvents yielded better alignment. For a draw ratio of 117%, increasing the concentration of acetone (poor PVA solvent) in water (good PVA solvent) from 0% to 70% decreased the FWHM from 65° to 50°. Vigolo et al. hypothesize that in a poorer solvent there is less sliding and the cohesion of the SWNT-polymer network is better [62].

Au: Please check the Appropriate citation of Fig. 11.2

The improved CNRS process has also been used to spin fibers from DNA stabilized SWNT dispersions [69]. Typical fiber dimensions are 50 cm in length and 20 to 30 μm. Young's modulus as high as 19 GPa, and tensile strength as high as 130 MPa have been achieved; these values are two to three times better than those achieved for fibers spun from the SWNT-SDS dispersions. However, the electrical resistivity of fibers produced from the DNA-stabilized dispersions was more than 50% greater than that of the fibers produced form the SDS-stabilized suspensions [69].

Baughman and coworkers at the University of Texas at Dallas have built on the CNRS work and developed a process for producing SWNT fibers, primarily from used HiPco SWNTs dispersed in aqueous lithium dodecyl sulfate with PVA as a coagulant [7,63,64]. In this process, the spinning dispersion is injected into a stream of coagulant that is flowing in a pipe coaxial with the spinning needle. The gel protofibers are wound onto a mandrel and then passed through a series of acetone and water baths for drawing and solvent removal. The gel protofibers can be continuously processed

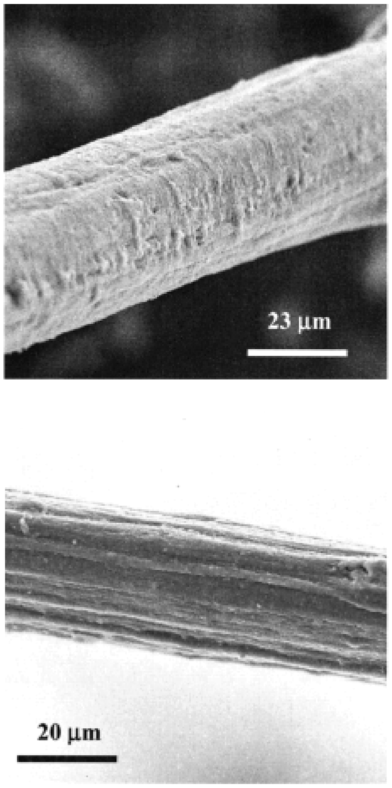

FIGURE 11.2 Effect of drying under load on alignment [62].

at approximately 100 cm/min to produce reels of several hundred continuous meters of 50 µm–diameter fibers consisting of approximately 60 wt% SWNT and 40% PVA [70]. Like Vigolo et al., Baughman et al. also found that HiPco tubes spin over a much broader concentration range and produced more mechanically robust ribbons [63].

The fibers have impressive mechanical and electrical actuation properties [64,70]. The PVA forms a coating on the SWNTs and the mechanical properties are believed to result from internanotube stress transfer via the PVA [70]. Tensile strengths up to 3.2 GPa have been achieved; this is nearly twice that of spider silk, and about ten times higher than that of the CNRS fibers. The Young's modulus is 80 GPa, which equals that of the fibers grown by Zhu et al. [23] and is double that of fibers spun by Vigolo et al. [62]; however, this value is still roughly an order of magnitude less than that of high-performance graphite fibers or individual SWNTs. Normalized for density, the Young's modulus and tensile strength of these fibers are more than twice that of steel and the fibers are approximately 20 times as tough as steel [64,70]. Fiber toughness, the total mechanical energy a specified mass of fiber absorbs before breaking, surpasses that of spider silk, the benchmark for fiber toughness. The predrawn SWNT/PVA fibers match the energy absorption of spider silk with a 30% breaking strain and continue to absorb energy until reaching an energy to break of over 600 J/g, which is higher than the best spider drag line silk (165 J/g) [70]. The high elongation required for toughness is achieved because the fiber does not neck during loading; testing showed that strain rate was linearly dependent on stress [64].

Dalton et al. [64] anticipate extending their technology to coagulation polymers other than PVA, particularly those with higher modulus or ionic conductivity. Initial commercial applications are anticipated in niche (low volume/high value) applications such as actuators for microcatheters for microsurgery, moving pins on dynamic braille displays, three dimensional optical fiber switches, and as a minority component for electronic textiles [64]. The ability to make the fibers into supercapacitors and weave them into textiles has been demonstrated; 100 micron supercapacitors provide high life cycle and comparable energy storage to large aqueous-electrolyte supercapacitors. However, the slower discharge rates indicate that higher fiber electrical conductivity must be achieved [70]. Other potential applications for weavable and sew SWNT/PVA fibers are distributed sensors, electronic interconnects, electromagnetic shields, antennas, and batteries [64]. Fiber toughness could be exploited in antimeteorite/antiballistic shields for satellites, antiballistic vests, and explosion-proof blankets for aircraft cargo bays. Longer term applications include actuators (artificial muscles) for prosthetics and severe environments such as those encountered in planetary exploration and aircraft engines [70].

11.4.2.3 Fibers Produced from SWNT/Superacid Dispersions

Highly aligned fibers consisting solely of SWNTs have been produced by wet-spinning SWNT/superacid dispersions [37,45,71,72]. The direct protonation of single-wall carbon nanotubes in superacids allows them to be dispersed at more than an order of magnitude higher concentration than that typically achieved in surfactants or organic solvents [37–39,72]. Rheology and microscopy show that SWNTs in superacids roughly parallel the phase behavior of rod-like polymer solutions (such as PPTA in sulfuric acid) used for solution spinning of high-performance fibers from nematic liquid crystals [37].

The phase behavior of rod-like polymer solutions is depicted in Fig. 11.3. With increasing concentration, such systems transition from a dilute solution where individual rods do not interact with each other, to a semidilute solution where rotation is inhibited, to an isotropic concentrated solution where both translation and rotation

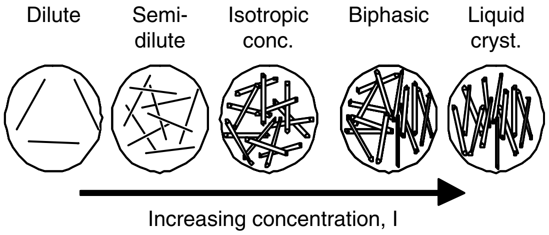

FIGURE 11.3 Phase behavior of rigid rods in solution [37].

are inhibited. At concentrations above the percolation threshold, steric effects cause the system to phase separately into a liquid crystalline phase in equilibrium with the isotropic concentrated phase [73,74]. Raising the concentration further increases the proportion of the liquid crystalline phase until the system becomes fully liquid crystalline.

In superacids, SWNTs form charge-transfer complexes of positively charged nanotubes surrounded by acid anions [38]. Such charge-transfer complexes repel each other electrostatically at short distance; however, the charges are screened by the acid (which is fully dissociated); thus electrostatic repulsion is expected to decay rapidly with SWNT separation, and the SWNTs can attract each other at longer separation distances through van der Waals forces (which have long range in the case of long, finite-diameter cylinders [65] such as SWNTs). Such long-range forces, together with excluded volume, seem responsible [75] for the inception of the spaghetti phase at much lower concentration than would be predicted by the theory for noninteracting rods [37]. The spaghetti phase consists of aligned, mobile SWNTs/acid charge-transfer complexes surrounded by sulfuric acid anions. At high enough concentration (approximately 4 wt% SWNT for purified [54] HiPco SWNTs with an average aspect ratio L/D of 470 dispersed in 102% sulfuric acid), the SWNT spaghetti coalesce forming a nematic liquid crystal. This liquid crystal has a birefringent polydomain structure and key rheological signatures such as a maximum in the viscosity versus concentration curve, long oscillatory transients, and the first normal stress difference changing sign from positive to negative and back to positive with increasing shear rate [37]. Moreover a variety of aligned species can be formed from the dispersion. Liquid crystals of oxidized MWNTs [76] and SWNTs in isopropyl acrylamide gel [77] have also been reported.

Production of SWNT fibers from 102% H_2SO_4 requires mixing of the dispersion in an anhydrous environment. The introduction of moisture destabilizes the dispersion resulting in the formation of tactoid-shaped aggregates dubbed alewives, roughly 50 µm long and 2 µm wide [37,38,78]. The alignment in the dispersion facilitates the production of highly aligned neat SWNT fibers even in the absence of drawing. Simply pushing the dispersion through a 125-µm syringe needle into a diethyl ether coagulation bath results in the formation of fibers with 12 : 1 axial to radial alignment as measured by Raman spectroscopy [45]. The development of an integrated mixing and spinning apparatus for producing SWNT fibers from SWNT acid dispersions has resulted in fibers with better alignment and properties [45,72]. Fibers have been produced from 4 to 10 wt% purified SWNT in 102% sulfuric acid. The maximum achievable SWNT loading has been dictated by the ability to mix and extrude the dispersion. The viscosity of the 6 wt% dispersion is roughly 1000 Pa s at 0.1 s^{-1} (one million times that of water) at room temperature, and heating has little effect on the viscosity.

Typical coagulants for the SWNT/superacid dispersions are diethyl ether, dilute sulfuric acid solutions, and water. Diethyl ether is an effective coagulant for these fibers because it is miscible with sulfuric acid and it evaporates rapidly in air upon removal from the bath. During coagulation, the SWNTs do not have time to reorient and the fiber quickly collapses into a dense structure [45]. Both dilute sulfuric acid solutions and water facilitate mass transfer of the 102% sulfuric out of the fiber and result in a denser fiber of more uniform cross section. Water-coagulated fibers spun from 8 wt% SWNT in 102% H_2SO_4 had a density of 1.1 g/cc, approximately 77% of the theoretical close-packed density for 1.0 nm SWNTs (1.5 g/cc) [72]. In all cases annealing at high temperatures (on the order of 600 to 800°C) is needed to remove residual sulfur [13,72].

Scanning electron microscopy (SEM) of fibers produced from 6–10 wt% SWNT show significant alignment and a consistent, clean surface morphology generally free of impurities [37,45]. High-magnification images of the neat SWNT fibers reveal a fiber substructure of aligned SWNT bundles approximately 200–600 nm in diameter and a bundle substructure of ropes on the order of 20 nm [45,72]. The fibers possess a relatively uniform circular cross section, which indicates a homogenous coagulation without brittle skin formation or structural collapse. Peeling of the fibers as well as cross-sectioning of the fibers by microtome and UV-ozone etching [45,72,79] show that the alignment and packing are consistent throughout the fiber. This differs from the SWNT/PVA fibers where the surface is more aligned and has a different morphology than the interior [67].

Fiber alignment as high as 28 : 1 axial to perpendicular have been measured by polarized Raman spectroscopy; the fibers are the most highly aligned macroscopic neat SWNT material produced to date [45,80]. This alignment is achieved without any extensional drawing during fiber production; it is largely the result of the liquid crystalline nature of the SWNT/super acid dispersion. Zhou et al. determined that for 6 to 8 wt% purified SWNTs dispersed in 100% H_2SO_4 and spun into diethyl ether, decreasing extrusion orifice diameter from 500 to 125 μm improved alignment and electrical and thermal transport [13]. The improvement in alignment was quantified by the FWHM of wide-angle x-ray scattering peaks, decreasing from 63° to 45° and the aligned fraction as measured by Raman increasing from 0.83 to 0.94 [13]. Subsequent improvements in fiber spinning have resulted in even more highly aligned fibers (FWHM of 31°) [72]. Annealing the fibers at 1100°C in argon for 24 hours or at 1150°C in vacuum for 2 hours had little effect on the alignment. Annealing also had little to no effect on the thermal conductivity of the fibers. Thermal conductivities at 300 K were 17 W/mK and 5 W/mK for the most and least aligned fibers, respectively [13]. These low values, compared to that of graphite parallel to the layers, are likely the result of several factors. The cross-sectional area was based on the macroscopic dimensions and did not account for gross voids or porosity. Also the fibers are not perfectly aligned, and the gaps between bundles represent thermal barriers [13].

Unlike alignment and thermal conductivity, electrical properties were significantly affected by annealing. The as-produced fibers are heavily p-doped with low resistivity and metallic behavior above 300 K; resistivity decreased from 0.64 to 0.25 Ωm cm at 300 K for the 500- and 125-μm orifices, respectively. Annealing the fibers removed the residual acid dopants causing an order of magnitude increase in resistivity at 300 K and a nonmetallic temperature dependence [13]. Thermoelectric power (S) measurements show an unusual low-temperature behavior that is explained by a one-dimensional phonon-drag model [81]. The two characteristic features of a phonon-drag contribution are the upturn in the thermopower at $T_0 \approx 0.1\hbar\omega_Q/k_B$, where $\hbar\omega_Q$ is the energy of the relevant phonon mode, and a peak around $dS/dT \approx 2.3T_0$. The fibers from SWNT/acid show an upturn in thermopower at $T_0 = 26$ K and a differential temperature maximum at 49–55 K. Modeling the data by a sum of phonon drag thermopower and diffusion thermopower results in the phonon energy $\hbar\omega_Q = 0.01$ eV, diffusion thermopower coefficient $b = 0.04$ μV/K^2, and $L_{ph}(Q) = 0.5$ to 0.1 μm.

Fiber mechanical properties depend on SWNT concentration, orifice diameter (alignment), and coagulant. A Young's modulus of 120 GPa and tensile strengths of 120 MPa have been achieved in fibers on the order of 50 micrometers in diameter and tens of meters in length [72]. The tensile strength is limited by the presence of defects, voids, and rope-rope interfaces, and was improved by a factor of 30 over the course of one year [72]. Further optimization of the dispersion, spinning conditions, coagulation conditions, and postprocessing are expected to reduce fiber defects and improve mechanical properties.

11.5 CONCLUSION

The development of SWNT nanotube fibers is in its infancy, and the performance expected from the nanoscale properties of SWNTs has yet to be realized in macroscopic objects. However, preliminary composite and neat fibers show promising results. It is likely that spinning processes will evolve to meet specific applications' needs. SWNTs dispersed in a polymer matrix may be best suited for extending the potential applications of existing polymeric materials by enhancing thermal and electrical conductivity and compressive strength at a relatively low-cost differential. SWNT/surfactant dispersions may be solution spun for applications where toughness and other mechanical properties are most critical. SWNT/acid dispersions used to produce neat fibers may be best suited for applications with the most demanding thermal and electrical requirements. The development of these spinning technologies alongside with improvements in SWNT production, purification, and functionalization will undoubtedly result in a number of revolutionary fiber applications.

PROBLEMS

1. Describe a potential application for nanotube fibers. What properties would be required? What kind of nanotubes would you use? Which of the fiber production methods described in this section would you use? (At this stage, assume that cost is not an issue.)
2. How does the polydispersity in chirality, length, and diameter of SWNTs affect the different fiber spinning processes? How does this polydispersity affect fiber properties?
3. What are the biggest challenges in producing nanotube polymer composite fibers? How do these differ from the challenges in producing neat SWNT fibers?

ACKNOWLEDGMENTS

For discussions and for sharing ideas and experimental results we thank Lars Ericson, Sivarajan Ramesh, Rajesh Saini, Nick Parra-Vasquez, Hua Fan, Yuhuang Wang, Haiqeng Peng, Carter Kittrell, Bob Hauge, Wade Adams, Ed Billups, Boris Yakobson, Howard Schmidt, Wen-Fang Hwang, Rick Smalley, Satish Kumar, Karen Winey, Jack Fischer, Alan Dalton, Ray Baughman, Edgar Munoz, Philippe Poulin, and Erik Hobbie. We acknowledge funding from the DURINT initiative of the Office of Naval Research under Contract N00014-01-1-0789, from the Texas Advanced Technology Program through grant 003604-0113-2003, and from the National Science Foundation through Award EEC-0118007.

Au: Please provide a title for all journal articles and chapters in books.

REFERENCES

1. Tans, S.J., Devoret, M.H., Dai, H.J., Thess, A., Smalley, R.E., Geerligs, L.J., and Dekker, C., *Nature, 386,* 474–477, 1997.
2. Hone, J., Llaguno, M.C., Nemes, N.M., Johnson, A.T., Fischer, J.E., Walters, D.A., Casavant, M.J., Schmidt, J., and Smalley, R.E., *Appl. Phys. Lett., 77,* 666–668, 2000.
3. Berber, S., Kwon, Y.K., and Tomanek, D., *Phys. Rev. Lett., 84*, 4613–4616, 2000.
4. Hone, J., Whitney, M., Piskoti, C., and Zettl, A., *Phys. Rev. B, 59,* R2514–R2516, 1999.
5. Krishnan, A., Dujardin, E., Ebbesen, T.W., Yianilos, P.N., and Treacy, M.M.J., *Phys. Rev. B, 58,* 14013–14019, 1998.
6. Buongiorno-Nardelli, M., Yakobson, B.I., and Bernholc, J., *Phys. Rev. Lett., 81,* 4656–4659, 1998.
7. Baughman, R.H., Zakhidov, A.A., and de Heer, W.A., *Science, 297*, 787–792, 2002.
8. Zhang, X.F., Cao, A.Y., Li, Y.H., Xu, C.L., Liang, J., Wu, D.H., and Wei, B.Q., *Chem. Phys. Lett., 351,* 183–188, 2002.
9. Salvetat-Delmotte, J.P. and Rubio, A., *Carbon, 40,* 1729–1734, 2002.
10. Bronikowski, M.J., Willis, P.A., Colbert, D.T., Smith, K.A., and Smalley, R.E., *J. Vac. Sci. & Technol., A-Vac. Surf. and Films, 19,* 1800–1805, 2001.
11. Dai, H.J., *Carbon Nanotubes, 80,* 29–53, 2001.
12. Kitiyanan, B., Alvarez, W.E., Harwell, J.H., and Resasco, D.E., *Chem. Phys. Lett., 317,* 497–503, 2000.
13. Zhou, W., Vavro, J., Guthy, C., Winey, K.I., Fischer, J.E., Ericson, L.M., Ramesh, S., Saini, R., Davis, V.A., Kittrell, C., Pasquali, M., Hauge, R.H., and Smalley, R.E., *J. Appl. Phys., 95,* 649–655, 2004.
14. Yakobson, B.I. and Smalley, R.E., *Am. Scientist, 85,* 324–337, 1997.
15. Baughman, R.H., *Science, 290,* 1310–1311, 2000.
16. Baughman, R.H., *Science, 300,* 268–269, 2003.
17. De Zhang, W., Wen, Y., Liu, S.M., Tjiu, W.C., Xu, G.Q., and Gan, L.M., *Carbon, 40,* 1981–1989, 2002.
18. Thostenson, E.T., Ren, Z.F., and Chou, T.W., *Compos. Sci. Technol., 61,* 1899–1912, 2001.
19. Li, X.H., Zhang, J., Li, Q.W., Li, H.L., and Liu, Z.F., *Carbon, 41,* 598–601, 2003.
20. Li, Y.H., Wei, J.Q., Zhang, X.F., Xu, C.L., Wu, D.H., Lu, L., and Wei, B.Q., *Chem. Phys. Lett., 365,* 95–100, 2002.
21. Zhang, Y.G., Chang, A.L., Cao, J., Wang, Q., Kim, W., Li, Y.M., Morris, N., Yenilmez, E., Kong, J., and Dai, H.J., *Appl. Phys. Lett., 79,* 3155–3157, 2001.
22. Jiang, K.L., Li, Q.Q., and Fan, S.S., *Nature, 419,* 801–801, 2002.
23. Zhu, H.W., Xu, C.L., Wu, D.H., Wei, B.Q., Vajtai, R., and Ajayan, P.M., *Science, 296,* 884–886, 2002.
24. Wei, B.Q., Vajtai, R., Choi, Y.Y., Ajayan, P.M., Zhu, H.W., Xu, C.L., and Wu, D.H., *Nano Lett., 2,* 1105–1107, 2002.

25. Li, Y.L., Kinloch, I.A., and Windle, A.H., *Science, 304*, 276–278, 2004.
26. Gommans, H.H., Alldredge, J.W., Tashiro, H., Park, J., Magnuson, J., and Rinzler, A.G., *J. Appl. Phys., 88,* 2509–2514, 2000.
27. Griskey, R.G., *Polymer Process Engineering,* Chapman and Hall, New York, 1995.
28. Levich, V.G., *Physiochemical Hydrodynamics,* Prentice Hall, Englewood Cliffs, 1962.
29. Rakas, M.A., *The Effect of Coagulants on the Microstructure and Mechanical Properties of Lyotropic Fiber-Forming Polymers,* Department of Polymer Science and Polymer Engineering, University of Massachusetts, 1990 available through UMI.
30. Paul, D.R., *J. of Appl. Polym. Sci., 12,* 383–402, 1968.
31. Ziabicki, A., *Fundamentals of Fibre Formation, The Science of Fibre Spinning and Drawing,* John Wiley & Sons, London, 1976.
32. Hancock, T.A., Spruiell, J.E., and White, J.L., *J. Appl. Polym. Sci., 21,* 1227, 1977.
33. Hancock, T.A., *An Experimental and Theoretical Study of the Wet Spinning Process,* Department of Chemical Engineering, University of Tennessee: Knoxville, 1981; available through UMI, University of Tennessee, p. 168.
34. Chenevey, E.C. and Wadhwa, L.H., Technical Report AFWAL-TR-82-4194, Air Force Materials Laboratory, Dayton, 1982.
35. Berry, G.C., Wong, C.P., Venkatamen, S., and Chu, S.G., Technical Report: AFML-TR-79-4115, Air Force Materials Laboratory, Dayton, 1979.
36. Pottick, L.A., The Influence of Drying on the Structure and Mechanics of Poly (P-Phenylene Benzobisthiazole) Fibers (High Modulus/Strength, Dry-Jet Wet Spinning, Performance, Processing); Department of Polymer Science and Polymer Engineering, University of Massachusetts, 1986, available through UMI.
37. Davis, V.A., Ericson, L.M., Parra-Vasquez, A.N., Fan, H., Wang, Y., Prieto, V., Longoria, J.A., Ramesh, S., Saini, R., Kittrell, C., Billups, W.E., Adams, W.W., Hauge, R.H., Smalley, R.E., and Pasquali, M., *Macromolecules, 37,* 154–160, 2004.
38. Ramesh, S., Ericson, L.M., A. , D.V., Saini, R.K., Kittrell, C., Billups, W.E., Pasquali, M., Adams, W.W., Hauge, R.H., and Smalley, R.E., *J. Phys. Chem. B* 2004, web release date May 26, 2004.

Au: Please supply full last name.

39. Davis, V.A., Ericson, L.M., Saini, R., Sivarajan, R., Hauge, R.H., Smalley, R.E., and Pasquali, M., *Proceedings of the 2001 AIChE Annual Meeting,* Reno, NV, 2001.
40. Bahr, J.L., Mickelson, E.T., Bronikowski, M.J., Smalley, R.E., and Tour, J.M., *Chemical Communications, 2,* 193–194, 2001.
41. Georgakilas, V., Voulgaris, D., Vazquez, E., Prato, M., Guldi, D.M., Kukovecz, A., and Kuzmany, H., *J. Am. Chem. Soc., 124,* 14318–14319, 2002.
42. Saini, R.K., Chiang, I.W., Peng, H.Q., Smalley, R.E., Billups, W.E., Hauge, R.H., and Margrave, J.L., *J. Am. Chem. Soc., 125,* 3617–3621, 2003.
43. Ying, Y.M., Saini, R.K., Liang, F., Sadana, A.K., and Billups, W.E., *Org. Lett., 5,* 1471–1473, 2003.
44. Poulin, P., Vigolo, B., and Launois, P., *Carbon, 40,* 1741–1749, 2002.
45. Ericson, L.M., *Macroscopic Neat Single-Wall Carbon Nanotube Fibers,* Department of Applied Physics, Rice University, Houston, 2003, available through UMI.
46. Kiss, G.D., *Rheology and Rheo-Optics of Concentrated Solutions of Helical Polypeptides,* Department of Polymer Science and Polymer Engineering, University of Massachusetts, 1979, available through UMI.
47. Andrews, R.J., Rao, D., Rantell, A.M., Derbyshire, T., Chen, F., Chen, Y., J. Haddon, R.C, *Appl. Phys. Lett., 75,* 1329, 1999.

Au: Please verify author initials.

48. Haggenmueller, R., Gommans, H.H., Rinzler, A.G., Fischer, J.E., and Winey, K.I., *Chem. Phys. Lett., 330,* 219–225, 2000.

49. Van Hattum, F.W.J., Bernardo, C.A., Finegan, J.C., Tibbetts, G.G., Alig, R.L., and Lake, M.L., *Polym. Composites, 20,* 683–688, 1999.
50. Tibbetts, G.G. and McHugh, J.J., *J. Mater. Res., 14,* 2871–2880, 1999.
51. Lozano, K., Bonilla-Rios, J., and Barrera, E.V., *J. Appl. Polym. Sci., 80,* 1162–1172, 2001.
52. Ma, H.M., Zeng, J.J., Realff, M.L., Kumar, S., and Schiraldi, D.A., *Compos. Sci. Technol., 63,* 1617–1628, 2003.
53. Bhattacharyya, A.R., Sreekumar, T.V., Liu, T., Kumar, S., Ericson, L.M., Hauge, R.H., and Smalley, R.E., *Polymer, 44,* 2373–2377, 2003.
54. Chiang, I.W., Brinson, B.E., Huang, A.Y., Willis, P.A., Bronikowski, M.J., Margrave, J.L., Smalley, R.E., and Hauge, R.H., *J. Phys. Chem. B, 105,* 8297–8301, 2001.
55. Kitagawa, T., Ishitobi, M., and Yabuki, K., *J. Polym. Sci. B, 38,* 1605–1611, 2000.
56. Kumar, S., Dang, T.D., Arnold, F.E., Bhattacharyya, A.R., Min, B.G., Zhang, X.F., Vaia, R.A., Park, C., Adams, W.W., Hauge, R.H., Smalley, R.E., Ramesh, S., and Willis, P.A., *Macromolecules, 35,* 9039–9043, 2002.
57. Balberg, I., Anderson, C.H., Alexander, S., and Wagner, N., *Phys. Rev. B, 30,* 3933–3943, 1984.
58. Sreekumar, T.V., Liu, T., Min, B.G., Guo, H., Kumar, S., Hauge, R.H., and Smalley, R.E., *Adv. Mater., 16,* 58–61, 2004.
59. Liu, T., Sreekumar, T.V., Kumar, S., Hauge, R.H., and Smalley, R.E., *Carbon, 41,* 2440–2442, 2003.
60. Poulin, P., Vigolo, B., Penicaud, A., and Coulon, C., US2002/0102585 A1, Method for Obtaining Macroscopic Fibres and Strips from Colloidal Particles and in Particular Carbon Nanotubes, U.S.A., 2003.
61. Vigolo, B., Penicaud, A., Coulon, C., Sauder, C., Pailler, R., Journet, C., Bernier, P., and Poulin, P., *Science, 290,* 1331–1334, 2000.
62. Vigolo, B., Poulin, P., Lucas, M., Launois, P., and Bernier, P., *Appl. Phys. Lett., 81,* 1210–1212, 2002.
63. Lobovsky, A., Matrunich, J., Kozlov, M., Morris, R.C., Baughman, R.H., and Zakhidov, A.A., US 2002/0113335 A1, Spinning, Processing, and Applications of Carbon Nanotube Filaments, Ribbons and Yarns, 2002.
64. Dalton, A.B., Collins, S., Munoz, E., Razal, J.M., Ebron, V.H., Ferraris, J.P., Coleman, J.N., Kim, B.G., and Baughman, R.H., *Nature, 423,* 703–703, 2003.
65. Israelchvili, J.N., *Intermolecular and Surface Forces,* 2nd ed., Academic Press, London, 1992.
66. Hiemenz, P.C. and Rajagopalan, R., *Principles of Colloid and Surface Chemistry,* Marcel Dekker, New York, 1997.
67. Neimark, A.V., Ruetsch, S., Kornev, K.G., and Ravikovitch, P.I., *Nano Lett., 3,* 419–423, 2003.
68. Nativ-Roth, E., Levi-Kalisman, Y., Regev, O., and Yerushalmi-Rozen, R., *J. Polym. Eng., 22,* 353–368, 2002.
69. Barisci, J.N., Tahhan, M., Wallace, G.G., Badaire, S., Vaugien, T., Maugey, M., and Poulin, P., *Advanced Functional Mater., 14,* 133–138, 2004.
70. Dalton, A.B., Collins, S., Razal, J., Munoz, E., Ebron, V.H., Kim, B.G., Coleman, J.N., Ferraris, J.P., and Baughman, R.H., *J. Mater. Chem., 14,* 1–3, 2004.
71. Smalley, R.E., Saini, R., Sivarajan, R., Hauge, R.H., Davis, V.A., Pasquali, M., Ericson, L.M., US2003/0170166A1, Fibers of Aligned Single-Wall Carbon Nanotubes and Process for Making the Same, William Marsh Rice University, U.S.A., 2003.

72. Ericson, L.M., Fan, H., Peng, H.Q., Davis, V.A., Zhou, W., Sulpizio, J., Wang, Y., Booker, R., Ramesh, S., Saini, R., Kittrell, C., Lavin, G., Schmidt, H., Adams, W.W., Billups, W.E., Pasquali, M., Hwang, W.-F., Hauge, R.H., Fischer, J.E., Smalley. *submitted* 2004.
73. Onsager, L., *Ann. N.Y. Acad. Sci., 51,* 627, 1949.
74. Flory, P.J., *Proc. Royal Soc. London, Ser. A, 234,* 1956.
75. Lee, C. S. and Yakobson, B.I., in preparation.
76. Song, W.H., Kinloch, I.A., and Windle, A.H., *Science, 302,* 1363–1363, 2003.
77. Islam, M.F., Alsayed, A.M., Dogic, Z., Zhang, J., Lubensky, T.C., and Yodh, A.G., *Phys. Rev. Lett., 92,* 2004.
78. Saini, R., Sivarajan, R., Hauge, R.H., Davis, V.A., Pasquali, M., Ericson, L.M., Kumar, S., Veedu, S., US2003/0133865A1, Single-Wall Carbon Nanotube Alewives, Process for Making and Compositions Thereof, William Marsh Rice University, U.S.A., 2003.
79. Wang, Y. et al., in preparation.
80. Walters, D.A., Casavant, M.J., Qin, X.C., Huffman, C.B., Boul, P.J., Ericson, L.M., Haroz, E.H., O'Connell, M.J., Smith, K., Colbert, D.T., and Smalley, R.E., *Chem. Phys. Lett., 338,* 14–20, 2001.
81. Vavro, J., Llaguno, M.C., Fischer, J.E., Ramesh, S., Saini, R.K., Ericson, L.M., Davis, V.A., and Smalley, R.E., *Appl. Phys. Lett.,* 2003.

Au: Please supply volume or issue